SSC BEAM PROFILE FROM SYNCHROTRON RADIATION

PART I: RESOLUTION ISSUES

Donald H. Stork
SSC Central Design Group
April 28, 1986

A. Introduction.

The very high energies at the SSC provide unique oportunities for detailed beam profile measurements to be made in a non-destructive manner by focusing synchrotron radiation on a sensitive, finely-segmented detector. Before evaluating the selection, installation, and operation of an appropriate optical system and detector, we must understand the special character of the spectral and angular intensity distributions of the synchrotron radiation at the SSC. We investigate in Part I the constraints on resolution imposed by geometry, by diffraction effects, and by the nature of the synchrotron radiation itself. In Part II we will investigate the spectral and angular intensity distributions. An evaluation of potential optical systems and detectors will be carried out by simulation techniques in Part III.

B. Characteristics of Synchrotron Radiation.

Synchrotron radiation is caused by the acceleration of an electric charge moving in a magnetic field. The power radiated by a relativistic particle increases, for given radius of curvature ρ, with the fourth power of the particle energy[1] :

$$P = \frac{2}{3}\alpha\frac{\hbar c^2}{\rho^2}\beta^3\gamma^4.$$

The power radiated by a proton which has a 10.1 kilometer radius of curvature (CDR[2] : 20 TeV, 6.6T) is plotted as a function of proton energy in Figure 1.

Synchrotron radiation in a constant magnetic field is a familiar phenomenon. The "critical energy", the photon energy above which half the power is radiated, is[3]

$$E_c = \frac{3}{2}\frac{\hbar c}{\rho}\gamma^3.$$

The critical energy is plotted as a function of SSC beam energy in Figure 2. The corresponding wavelengths can be determined from the plot of photon wavelength versus photon energy in Figure 3. At 20 TeV, $E_c = 280 eV$ (and $P = 8.5$ Watts for the two rings at design current). At 1 TeV, $E_c = 0.035$ eV and synchrotron radiation can not be detected coming from the constant field regions.
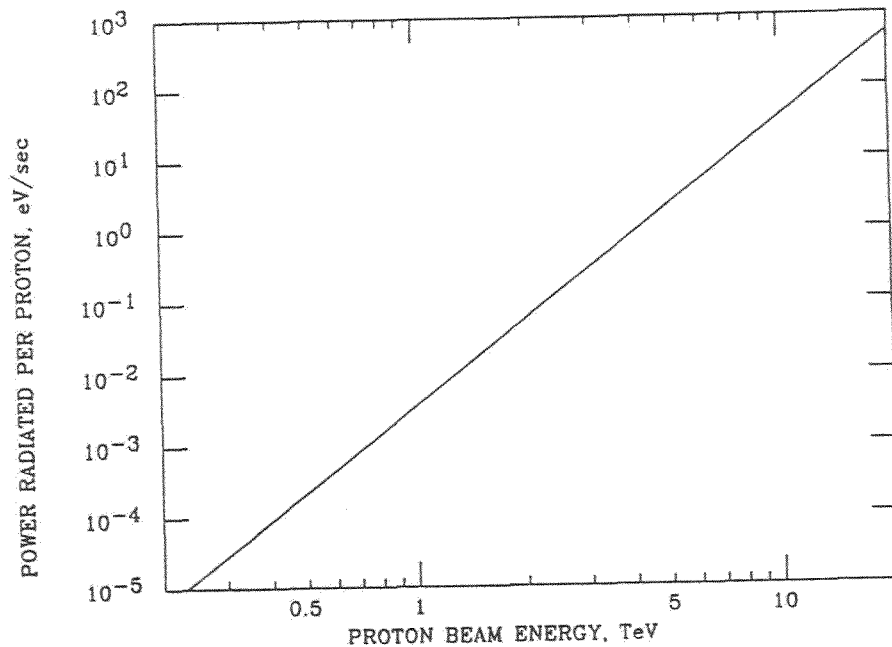
1. Synchrotron radiation power radiated by a proton in a constant magnetic field for radius of curvature 10.1 km (CDR design for horizontal dipoles) as a function of proton energy.
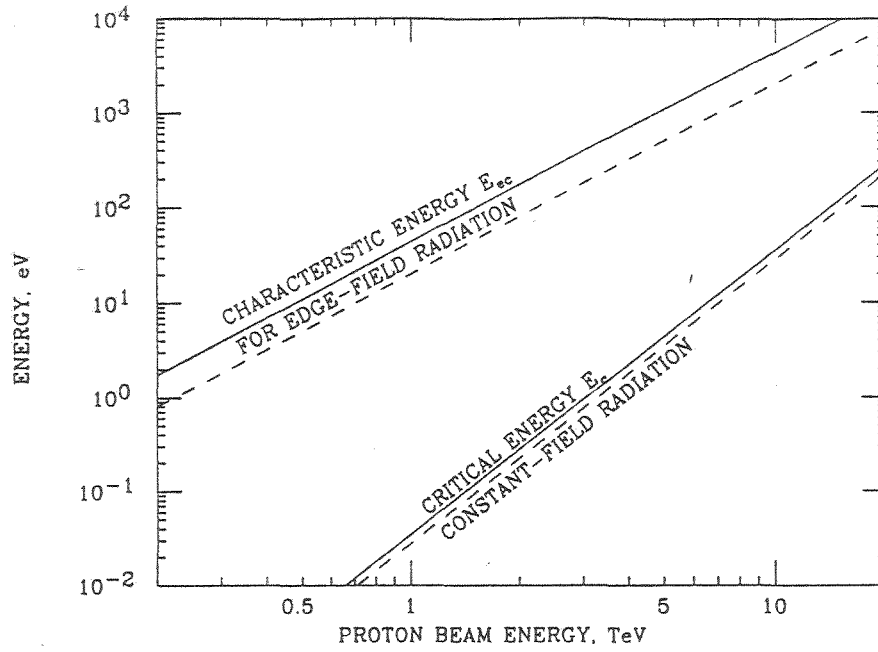
2. "Critical" energy $E_c = 1.5(\hbar c/\rho)\gamma^3$ for constant-field synchrotron radiation and "characteristic" energy $E_e c = 4\pi(\hbar c/L)\gamma^2$ for edge-field synchrotron radiation as a function of SSC beam energy. The solid/dashed curves are for the CDR horizontal/vertical dipole magnets.
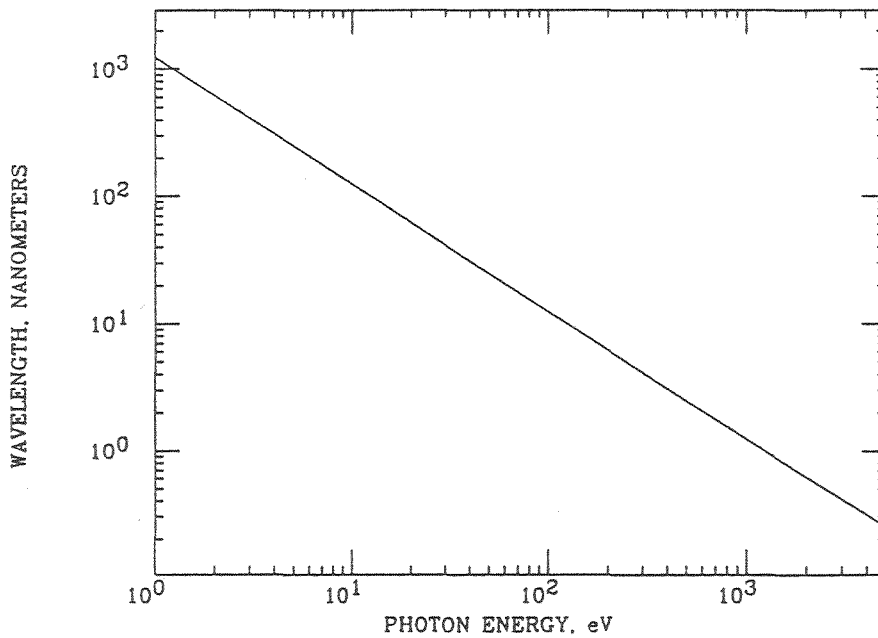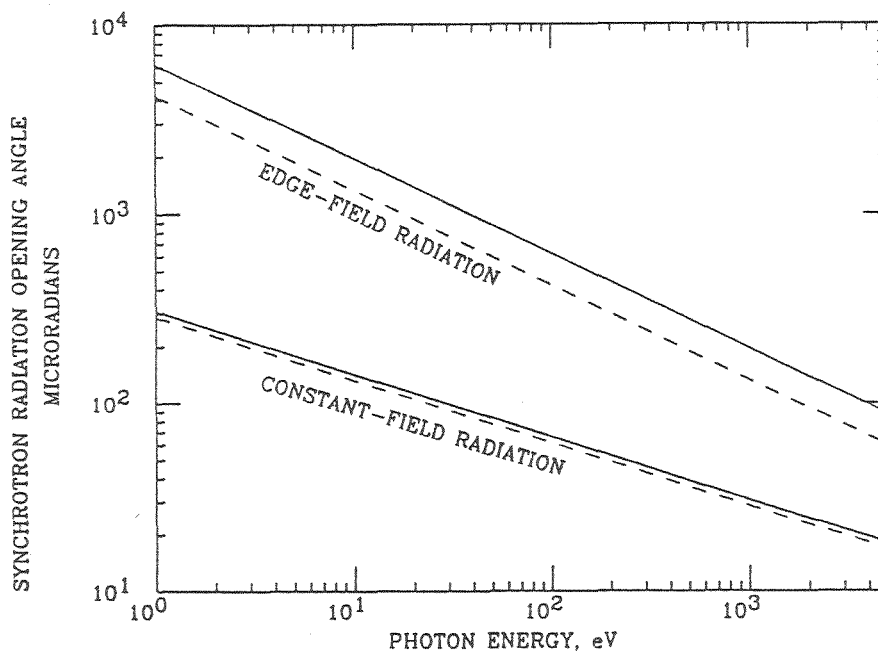

3. Photon wavelength as a function of photon energy.

The angular distribution for constant-field radiation is concentrated in the forward direction in an angular cone characterized by

$$\theta_S = \left(\frac{3\hbar c}{2\rho E_\gamma} \right)^{\frac{1}{3}}.$$

The angle θ_S is plotted as a function of photon energy E_γ in Figure 4. Note that the angular spread does not depend on particle energy—only on photon energy E_γ! However, as particle energy is increased, the spectral distribution moves to higher photon energies with a consequent increased collimation in the forward

4. Opening angle for constant-field and for edge-field synchrotron radiation as a function of photon energy. The solid/dashed curves are for the CDR horizontal/vertical dipole magnets.

direction. This is emphasized by the equivalent formula

$$\theta_S = \frac{1}{\gamma} \left(\frac{E_c}{E_\gamma} \right)^{\frac{1}{3}}$$

which shows that at critical energy, $\theta_S(E_c) = 1/\gamma$.

Less familiar is the character of synchrotron radiation from the edge-field region[4]. Particles entering or leaving a magnetic field region experience a variable acceleration for a very short time and the synchrotron radiation appears over an extended frequency range, although the power radiated is in accord with the equation above. A "characteristic" photon energy for this case[5] is

$$E_{ec} = 4\pi \frac{\hbar c}{L} \gamma^2$$

where L is a measure of the distance in which the field changes, about 6.5 cm for the present CDR SSC horizontal dipole design[6] and about 14.1 cm for the vertical dipoles. The characteristic photon energy is plotted for $L = 6.5$ and 14.1 cm as a function of SSC beam energy in Figure 2. The edge radiation at 1 TeV extends well into the visible region where detection is relatively straight forward.

The angular distribution for edge-field radiation is characterized by a typical opening angle[5]

$$\theta_{eS} = \left(\frac{2\lambda}{L} \right)^{\frac{1}{2}}.$$

θ_{eS} is plotted for the two values of L in Figure 4 as a function of photon energy. An equivalent expression is

$$\theta_{eS} = \frac{1}{\gamma} \left(\frac{E_{ec}}{E_\gamma} \right)^{\frac{1}{2}}.$$

At the characteristic edge-field photon energy, $\theta_{eS}(E_{ec}) = 1/\gamma = \theta_S(E_c)$. For given photon energy the edge-field radiation is broader than constant-field radiation, a fact that can be exploited in improved resolution in cases where the diffraction limit arises from the narrow synchrotron radiation cone.

5

C. SSC Geometry.

In the SSC geometry, radiation originating at or near the entrance edge of a horizontal dipole will be separated from the beam direction by 1.64 mr at the exit of the dipole. However, the spacial separation will be little more than a centimeter at exit and an additional 7 meters is required for a 25 mm separation. A lens or focusing mirror might be placed at this point, about 24 m from the source. If the optical aperture were 10 mm, as illustrated in Figure 5, the exit port would require a 7-m gash in a CDR 3.45-cm beam pipe or would require a 7-m long 6-cm diameter beam pipe section in order to maintain a 20 mm clearance between the optical system and beam centerline. For detection in the soft X-ray region, only small-angle reflections might be possible and the radiation channel might only gradually separate from the beam pipe. In this circumstance, only the last dipole in a string would be useful. Beta functions within the arcs vary
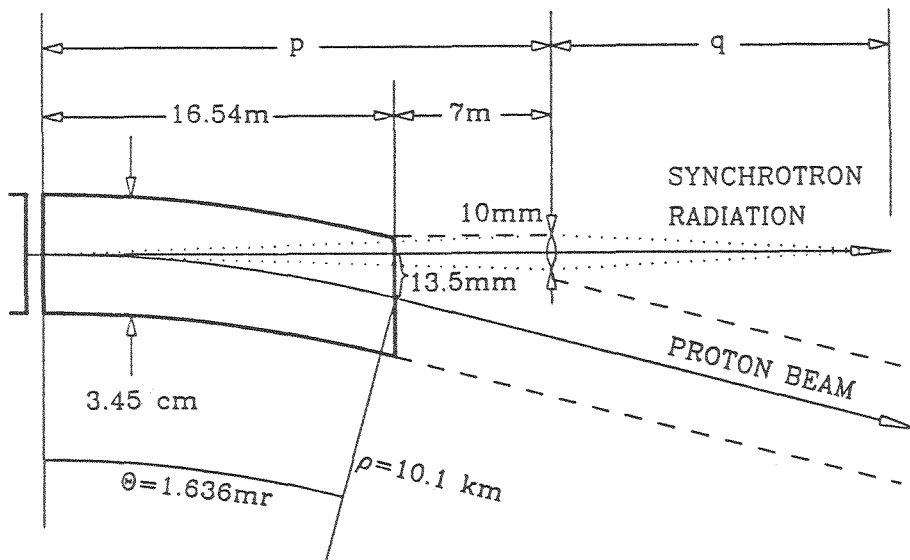
5. Geometry for synchrotron radiation from the last horizontal dipole in a string. A 10 mm lens is centered 25 mm to the side of beam center, 23.54 m downstream from the entrance field region and 24.34 m downstream from the previous exit field region.

between 111 and 332 meters[2] corresponding to rms transverse beam dimensions of about 320 to 560 microns for design emittance at 1 TeV and 72 to 125 microns at 20 TeV. Dimensions are slightly smaller at the point illustrated in Figure 5: about 310 to 500 microns at 1 TeV and 69 to 112 microns at 20 TeV for the last dipole toward an IR or utility straight in a dispersion supression string.

An alternative would be to use the vertical bending magnets near the interaction points. The CDR field is 5.212 T at 20 TeV corresponding to a radius of curvature of 12.8 kilometers. The geometry is illustrated in Figure 6. In the CDR geometry, the vertical bending magnets have 75 mm bore and the lens (or mirror) would have to be placed in a reentrant port to maintain the transverse beam clearance shown in the figure. In particular, the second pair of vertical
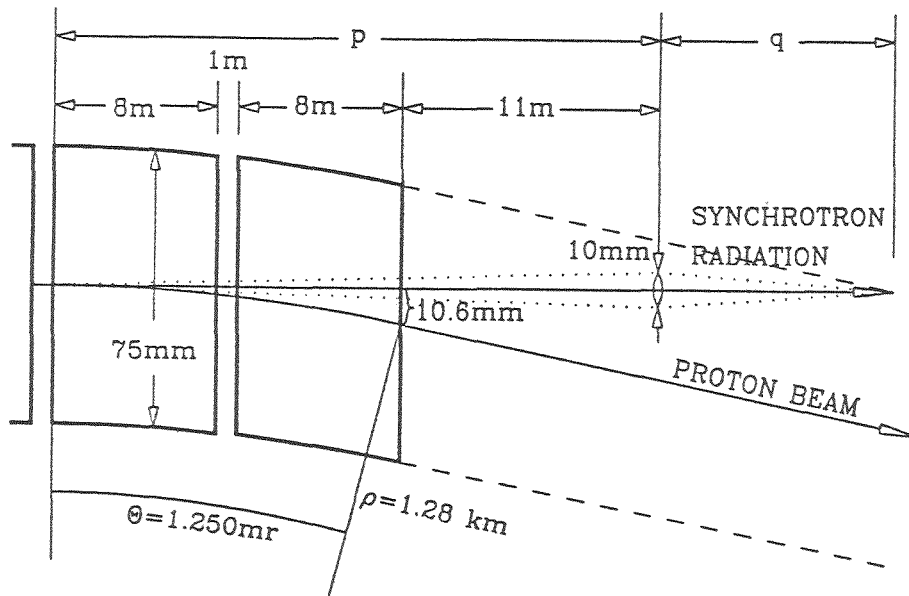
6. Geometry for synchrotron radiation from the last vertical dipole in a string. A 10 mm lens is centered 25 mm to the side of beam center, 28 m downstream in the forward direction from one entrance field region and 29 m downstream from the previous exit field region (if present).

bending magnets away from the high-beta interaction points has a beta close to 1 km with corresponding rms transverse beam dimensions of 900 to 1100 microns for 1 TeV and 210 to 250 microns for 20 TeV.

Some of the characteristics of synchrotron radiation for both horizontal and vertical bend magnets are shown in the following table for 1 and 20 TeV. A comparison is made to two electron colliders, SPEAR and PEP, and to the CERN SPP̄S collider at 270 GeV (edge field synchrotron radiation was first observed for protons for energies 290 to 400 GeV at the CERN SPS[7] .

	SPEAR	PEP	SPP̄S	TEV-I	SSC HBEND (VBEND)	SSC HBEND (VBEND)
E_{beam} (GeV)	4.2	14.5	270	800	1000	20000
γ	8219	28376	288	853	1078	21552
B (T)	1.15	0.292	1.215	3.536	0.330 (0.261)	6.60 (5.21)
ρ (m)	12.17	165.5	741	755	10109 (12805)	10109 (12805)
$\sigma_x, \sigma_y (\mu)$					314-494 (920-1133)	70-110 (206-253)
E_c (eV)	13504	39550	0.00013	0.00086	0.0355 (0.0280)	284 (224)
λ_c (nm)	0.092	0.0312	—	—	34800 (44100)	4.38 5.55
θ_S at E_c (μr)	122	35	—	—	928	46
L_{ec} (cm)			4.4	12.4	6.5 (14.1)	6.5 (14.1)
E_{ec} (eV)			4.67	14.5	44.3 (20.4)	17717 (8167)
λ_{ec} (eV)			262	84	27.6 (60)	0.069 (0.150)
θ_{eS} at E_{ec} (μr)			3472	1172	928	46

D. Geometric Optics.

Some of the peculiarities of the bend-plane (B) optics for synchrotron radiation from the constant field region are illustrated in Figure 7. The corresponding optics in the plane normal (N) to the bend plane are illustrated in Figure 8. The lens focuses synchrotron radiation from the object point B_1 (at object distance p) to the image point B_2 (at image distance q). A detector placed at B_2 can measure the transverse extent of the beam at B_1 to within the limits placed by curvature distortion, depth of field distortion, chromatic aberration, lens imperfections, detector resolution and diffractive effects. Desired source resolution ranges from 35 to 550 μ (half of σ_z, σ_y) depending upon beam energy and choice of horizontal or vertical bend magnets.
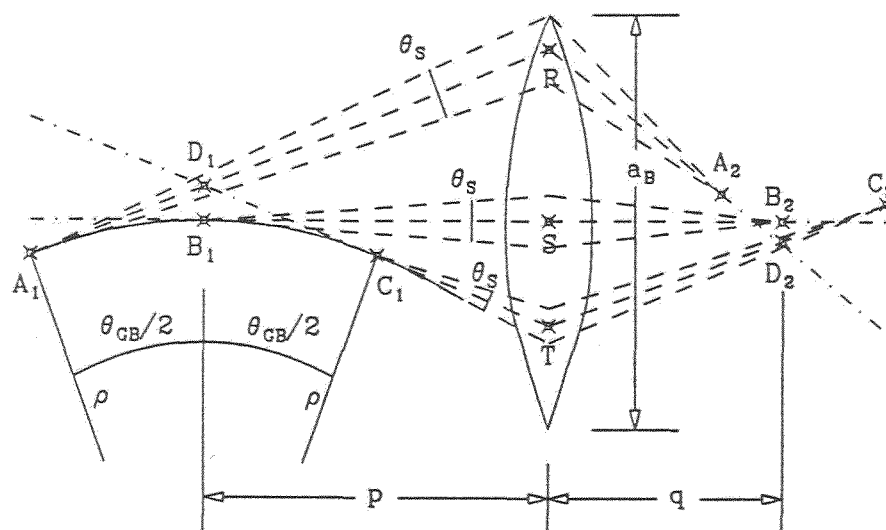
7. Illustration of focussing for a given wavelength of synchrotron radiation in the bend plane (B). The point B_1 at object distance p is focused to point B_2 at image distance q. Also shown are the object and image points for the ends of particle's arc trajectory of length θ_{GB}.

Problems peculiar to synchrotron radiation arise from the narrow forward radiation cone and from the curvature distortion caused by the bend of the radiating particle. In Figure 7 (in which $\theta_S \ll \theta_{GB}$) the curvature produces a spread of image B_2D_2 corresponding to a source spread B_1D_1. The intensity distribution across B_1D_1 is actually cusp-like as shown in Figure 9a with rms deviation

$$\sigma^B_{curv} = \frac{2}{3\sqrt{5}}B_1D_1 = \frac{2}{3\sqrt{5}}\frac{\rho\theta^2_{GB}}{8} = 0.0373\rho\theta^2_{GB} \qquad (\theta_S \ll \theta_{GB})$$
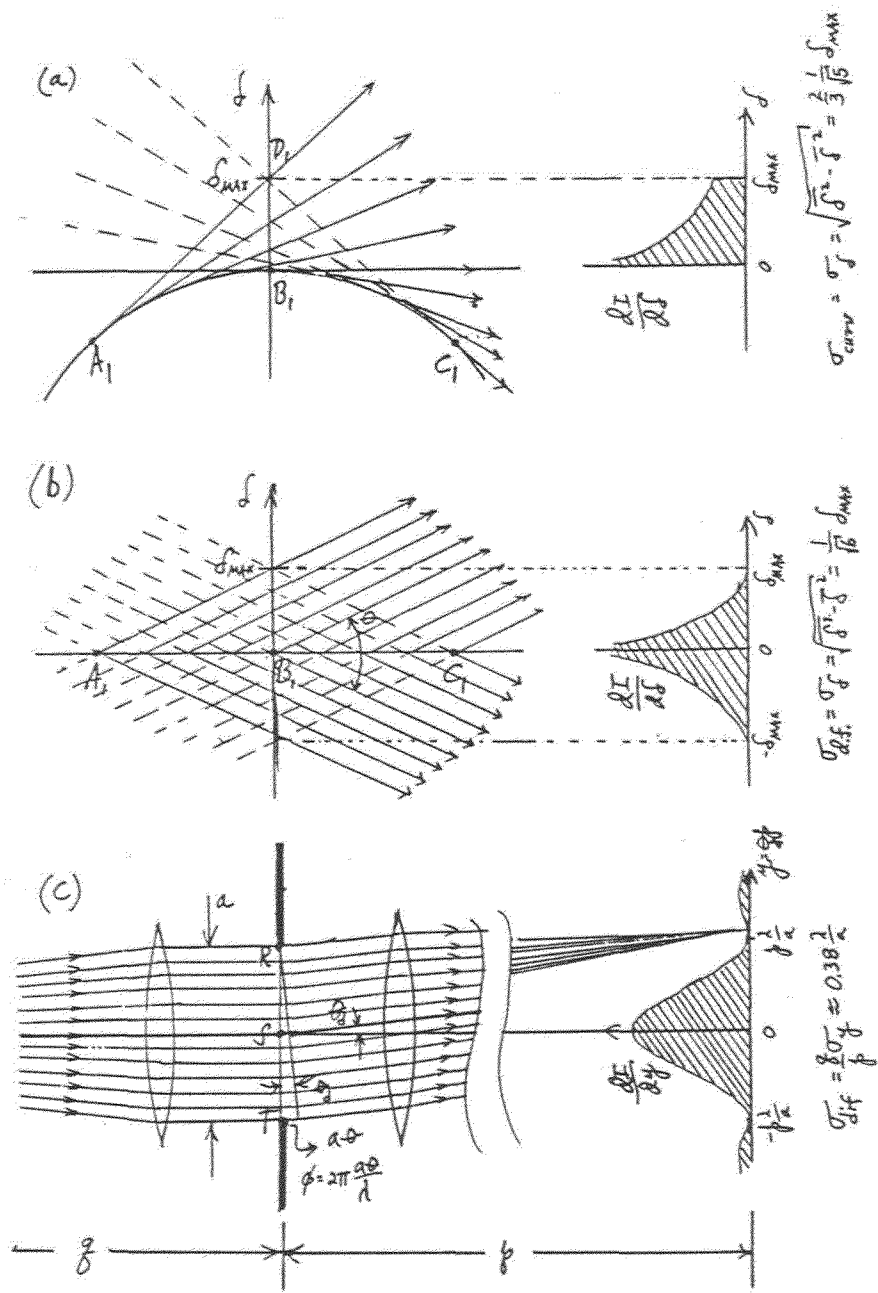
where

$$\theta_{GB} = \frac{a_B}{p},$$

a_B being the bend-plane lens aperture and p the distance from source to lens.
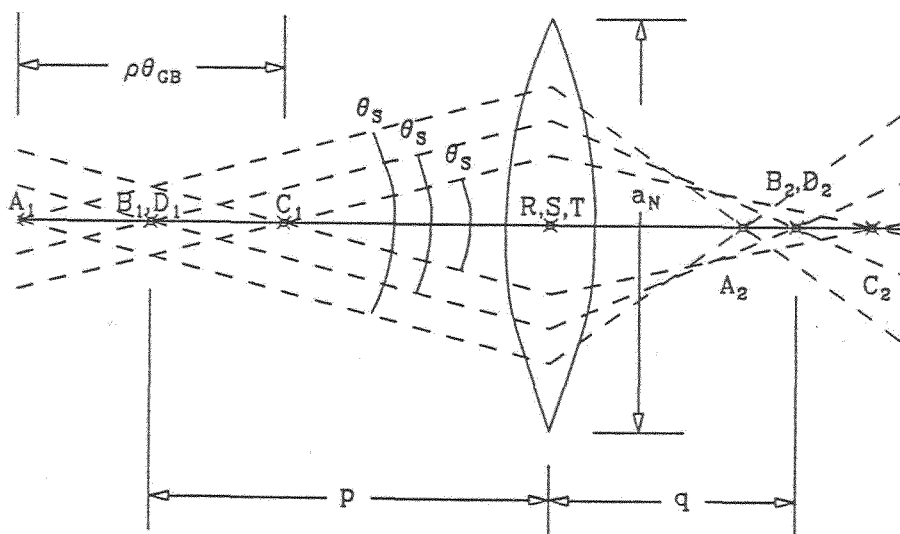
8. Illustration of focusing of synchrotron radiation in the plane normal (N) to the bend plane. The labelled points correspond to those in Figure 7.

9. Illustration of the effects that limit resolution. In each case, the effect is described by a "σ" which is the rms transverse deviation from the mean of the apparent source intensity distribution. (a) Curvature distortion (a pencil beam produced tangentially to each point on the arc: σ_{curv}. (b) Depth-of-field distortion (source points along the line A_1B_1 fill the lens aperture θ_G or are limited by θ_S): $\sigma_{d.f.}$. (c) Diffraction distortion (for a one-dimensional slit):σ_{dif}.

11

If, on the other hand, the spread in synchrotron radiation angles is much greater than the angular aperture of the lens, then radiation is collected over an arc length $\rho\theta_S$ (instead of $\rho\theta_{GB}$) and the aberation is dominated by a depth of field effect. In Figure 8, which illustrates the optics in the plane perpendicular to the bend plane, the depth of field effect is obvious as a "circle of confusion" about the source position B1 with transverse extent $(A_1C_1/2)\theta_S$. With the arc length limited by $\rho\theta_{GB}$ as depicted in Figure 7, the depth of field resolution limit in the plane normal (N) to the bend plane contributes an rms spread (see Figure 9b)

$$\sigma_{d.f.}^{N} = \frac{1}{\sqrt{6}}\frac{A_1C_1}{2}\theta_S = \frac{\rho\theta_{GB}\theta_S}{2\sqrt{6}} = 0.204\rho\theta_{GB}\theta_S \qquad (\theta_S \ll \theta_{GB}, \theta_S \ll \theta_{GN})\,.$$

If the arc length is limited by θ_S instead of bend-plane lens aperture, the depth of field resolution limit becomes

$$\sigma_{d.f.}^{N} = \frac{1}{\sqrt{6}}\frac{A_1C_1}{2}\theta_S = \frac{\rho\theta_S^2}{2\sqrt{6}} = 0.204\rho\theta_S^2 \qquad (\theta_S \gg \theta_{GB}, \theta_S \ll \theta_{GN})\,.$$

There are two more limiting cases for $\theta_S \gg \theta_{GN}$ where θ_{GN} is the angular lens aperture in the plane normal to the bend plane:

$$\sigma_{d.f.}^{N} = \frac{1}{\sqrt{6}}\frac{A_1C_1}{2}\theta_{GN} = \frac{\rho\theta_{GB}\theta_{GN}}{2\sqrt{6}} = 0.204\rho\theta_{GB}\theta_{GN} \quad (\theta_S \ll \theta_{GB}, \theta_S \gg \theta_{GN})\,,$$

$$\sigma_{d.f.}^{N} = \frac{1}{\sqrt{6}}\frac{A_1C_1}{2}\theta_{GN} = \frac{\rho\theta_S\theta_{GN}}{2\sqrt{6}} = 0.204\rho\theta_S\theta_{GN} \qquad (\theta_S \gg \theta_{GB}, \theta_S \gg \theta_{GN})\,.$$

In the horizontal plane, the corresponding normal depth of field resolution (in addition to the curvature distortion effect!) is, for limiting values of θ_{GB},

$$\sigma_{d.f.}^{B} = \frac{1}{\sqrt{6}}\left(\frac{A_1C_1}{2}\right)\theta_S = \frac{\rho\theta_{GB}\theta_S}{2\sqrt{6}} = 0.204\rho\theta_{GB}\theta_S \qquad (\theta_S \ll \theta_{GB})\,,$$

$$\sigma_{d.f.}^{B} = \frac{1}{\sqrt{6}}\left(\frac{A_1C_1}{2}\right)\theta_{GB} = \frac{\rho\theta_S\theta_{GB}}{2\sqrt{6}} = 0.204\rho\theta_S\theta_{GB} \qquad (\theta_S \gg \theta_{GB})\,.$$

Finally, to return to the curvature distortion, in the limit of small geometric

aperture

$$\sigma^B_{curv} = \frac{2}{3\sqrt{5}} B_1 D_1 = \frac{2}{3\sqrt{5}} \frac{\rho\theta_S^2}{8} = 0.0373\rho\theta_S^2 \qquad (\theta_S \gg \theta_{GB}) .$$

The above is for constant-field radiation where the depth of field and arc length are determined by $\rho\theta$. In the edge-field radiation case the depth of field and arc length are fixed by L, the effective edge-field thickness (and the effective radius of curvature is half of the central field value: $\rho = \rho_0/2$). Otherwise the considerations are the same leading to

$$\sigma^B_{curv} = \frac{2}{3\sqrt{5}} \frac{L^2}{8(\rho_0/2)} = 0.0745\frac{L^2}{\rho_0};$$

$$\sigma^B_{d.f.} = \frac{1}{\sqrt{6}} \frac{L}{2}\theta_{eS} = 0.204L\theta_{eS} \qquad (\theta_{eS} \ll \theta_{GB});$$

$$\sigma^B_{d.f.} = \frac{1}{\sqrt{6}} \frac{L}{2}\theta_{GB} = 0.204L\theta_{GB} \qquad (\theta_{eS} \gg \theta_{GB});$$

$$\sigma^N_{d.f.} = \frac{1}{\sqrt{6}} \frac{L}{2}\theta_{eS} = 0.204L\theta_{eS} \qquad (\theta_{eS} \ll \theta_{GN});$$

$$\sigma^N_{d.f.} = \frac{1}{\sqrt{6}} \frac{L}{2}\theta_{GN} = 0.204L\theta_{GN} \qquad (\theta_{eS} \gg \theta_{GN}).$$

E. Diffraction Limit.

Under ordinary circumstances light from each source point uniformly fills the geometric angular aperture $\theta_G = a/p$. The diffractive limit of angular resolution for geometric aperture a is then characterized by

$$\theta_{dif} = \frac{\lambda}{a} \qquad (\theta_S \gg \theta_G)$$

where

$$\lambda = 2\pi \left(\frac{\hbar c}{E_\gamma} \right)$$

is the wavelength of the synchrotron radiation for energy E_γ (see Figure 3, or recall that $2\pi\hbar c = 1244$ eV–nm). The diffraction resolution limit in the transverse

source dimension for this case has rms deviation

$$\sigma_{dif} = Fp\theta_{dif} = F\frac{\lambda}{\theta_G} \qquad (\theta_S \gg \theta_G).$$

The factor F is a form factor of order one. If we were concerned with the "Rayleigh criterion" for image resolution instead of rms transverse deviation, F would be 1.22 (corresponding to about a three standard separation separation between point sources). We desire here that our measure be rms deviation from the mean of the projected distribution, illustrated in Figure 9c, because we are interested in measuring projected beam profile distributions and can readily compare rms deviations. Thus, for this case[8], $F = 0.38$.

If, however, the forward synchrotron radiation cone, θ_S, is more tightly collimated, only a central part of the aperture is effectively illuminated:

$$a_S = p\theta_S$$

and the measure of the diffractive limit of angular resolution is now determined by

$$\theta_{dif} = \frac{\lambda}{a_S} \qquad (\theta_S \ll \theta_G),$$

and the diffraction resolution limit in the transverse source dimension becomes

$$\sigma_{dif} = F_S p\theta_{dif} = F_S \frac{\lambda}{\theta_S} \qquad (\theta_S \ll \theta_G).$$

Note that in the latter case σ_{dif} is independent of the distance p from source to lens. For constant-field radiation one can use the definition of θ_s and eliminate λ:

$$\sigma_{dif} = F_S \frac{\lambda}{\theta_S} = F_S \left(\frac{4\pi}{3}\right)^3 \rho\theta_S^2 = 73.5 F_S \rho\theta_S^2 \qquad (\theta_S \ll \theta_G).$$

And for comparison with the other limiting case:

$$\sigma_{dif} = F\left(\frac{\lambda}{\theta_G}\right) = 73.5 F_S \rho\theta_S^2 \left(\frac{F\theta_S}{F_S\theta_G}\right) \qquad (\theta_S \gg \theta_G).$$

The form factor F_S is now more complicated. It depends on the detailed

14

distribution of synchrotron radiation across the lens, whereas F above is for a uniformly illuminated aperture. Hofmann[5] has investigated the case for the synchrotron radiation distribution normal to the bend plane for $E_\gamma = 0.01 E_c$, (a limit of interest for electron machines, if not for proton beams). He finds a form factor "f_r" $= 0.5$ for the resolution requirement that the separation of two point sources produces a 2/3 midpoint intensity depression. Inspection of his diffraction distribution gives $F_S = 0.34$ for our rms transverse source distribution (albeit for $E_\gamma = 0.01 E_c$).

For edge-field radiation we find for diffraction limit by θ_{eS}

$$\sigma_{dif} = F_{eS} \left(\frac{\lambda}{\theta_{eS}} \right) = F_{eS} \left(\frac{L}{2} \right) \theta_{eS} \qquad (\theta_{eS} \ll \theta_G)$$

where the wavelength is eliminated by using the definition of θ_{eS}. If the diffraction limit is instead that of the geometric aperture,

$$\sigma_{dif} = F \left(\frac{\lambda}{\theta_G} \right) = F_{eS} \left(\frac{L}{2} \right) \theta_{eS} \left(\frac{F \theta_{eS}}{F_{eS} \theta_G} \right) \qquad (\theta_{eS} \gg \theta_G).$$

The form factors are different from those for constant-field radiation and, in fact, the form factors F_{eS}^B and F_{eS}^N are different. In our conclusions below, we will presume that these differences are not large and that all the form factors are close to 0.34. A detailed investigation of this point will be deferred to Part II.

The diffraction resolution at the source, σ_{dif} as determined by diffraction through $F = 0.38$ geometric apertures of 1, 2, 5, 10, and 20 mm at a distance of 30 meters is plotted as a function of photon energy in Figure 10. Also shown are large aperture $F_S = 0.34$ synchrotron radiation diffractive limits for constant- and edge-field sources, also at a distance of 30 meters.

F. Constant-Field Radiation and Beam Profile Resolution Limits:

Resolution in the bend plane is limited not only by diffractive effects but also by the depth of field along the curved particle path. Resolution in the plane

normal to the bend plane is limited not only by the aperture in the normal plane but by the length of arc accepted by the bend-plane optics. The various limiting contributions to the resolution are listed in the following table.

	$\theta_S \ll \theta_{GB}$ $\theta_S \ll \theta_{GN}$	$\theta_S \ll \theta_{GB}$ $\theta_S \gg \theta_{GN}$	$\theta_S \gg \theta_{GB}$ $\theta_S \ll \theta_{GN}$	$\theta_S \gg \theta_{GB}$ $\theta_S \gg \theta_{GN}$
$\rho\theta$	$\rho\theta_{GB}$	←same	$\rho\theta_S$	←same
σ_{dif}^B	$73.5 F_S^B \rho\theta_S^2$	←same	$73.5 F_S^B \rho\theta_S^2 \left(\dfrac{F^B\theta_S}{F_S^B\theta_{GN}}\right)$	←same
σ_{curv}^B	$0.0373\rho\theta_{GB}^2$	←same	$0.0373\rho\theta_S^2$	←same
$\sigma_{d.f.}^B$	$0.204\rho\theta_{GB}\theta_S$	←same	$0.204\rho\theta_S\theta_{GB}$	←same
σ_{dif}^N	$73.5 F_S^N \rho\theta_S^2$	$73.5 F_S^N \rho\theta_S^2 \left(\dfrac{F^N\theta_S}{F_S^N\theta_{GN}}\right)$	$73.5 F_S^N \rho\theta_S^2$	$73.5 F_S^N \rho\theta_S^2 \left(\dfrac{F^N\theta_S}{F_S^N\theta_{GN}}\right)$
$\sigma_{d.f.}^N$	$0.204\rho\theta_{GB}\theta_S$	$0.204\rho\theta_{GB}\theta_{GN}$	$0.204\rho\theta_S^2$	$0.204\rho\theta_S\theta_{GN}$
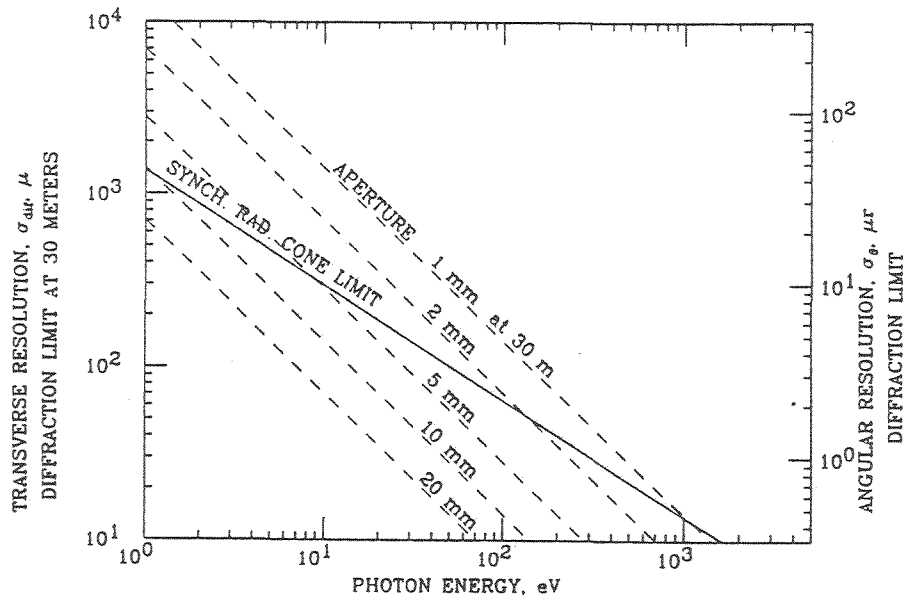
10. Diffractive limit of angular resolution. The dashed lines correspond to diffraction in geometric apertures of 1, 2, 4, 10, and 20 mm. The solid curve is for diffraction in an aperture determined by the synchrotron radiation characteristic opening angle at a distance of 30 meters.

It is now clear how to procede in optimizing beam profile resolution. The parameters that are available are θ_S (or λ), and the geometric apertures in the two planes.

If only the resolution in the plane normal to the bend plane is to be optimized, then for given wavelength λ the diffraction resolution can be improved by increasing the lens aperture θ_{GN} until it significantly exceeds θ_S.

$$\frac{\theta_{GN}}{F^N} \gg \frac{\theta_S}{F_S^N} \qquad \text{(diffraction condition)}.$$

Then the depth-of-field distortion in this plane can be kept at a significantly lesser level, provided

$$\theta_{GB} \ll \frac{73.5}{0.204} F_S^N \theta_S \qquad \text{(depth of field condition)}.$$

Clearly, θ_{GN} and θ_{GB} can be chosen to satisfy these conditions.

If only the bend-plane resolution is to be optimized, then the diffraction limit is improved by increasing the geometrical aperture θ_{GB} until it significantly exceeds the synchrotron radiation spread θ_S.

$$\frac{\theta_{GB}}{F^B} \gg \frac{\theta_S}{F_S^B} \qquad \text{(diffraction condition)}$$

However, if θ_{GB} can be kept small enough, the curvature and depth of field distortions can be kept well below the diffraction limit:

$$\theta_{GB} \ll \left(\frac{73.5}{0.0373} \right) F_S^B \theta_S \qquad \text{(curvature condition)};$$

$$\theta_{GB} \ll \left(\frac{73.5}{0.204} F_S^B \right)^{\frac{1}{2}} \theta_S \qquad \text{(depth of field condition)}.$$

The latter places the more stringent upper limit for reasonable values of F_S^B: if $F_S^B = .34$, then $\theta_{GB} \ll 11\theta_S$. In any case, it appears possible to choose a θ_{GB} that reasonably satisfies these conditions.

The requirements for best resolution in both planes are mutually consistent. With the appropriate choice of apertures, the resolution in both planes is diffraction limited by the narrow synchrotron radiation angular cone. Resolution and aperture requirements are illustrated in the table below for the case p = 30 meters and for $F_S^B = F_S^N = 0.34$.

E_γ (eV)	λ (nm)	θ_S (μr)	$\rho\theta_S$ (m)	$\sigma_{dif}^{B(N)}$ (μ)	a_B (mm)	a_B, a_N (mm)
2.5	500	228	2.30	747	< 166	> 6.84
25	50	106	1.07	160	< 77.1	> 3.18
250	5	49.1	0.50	35	< 35.6	> 1.47
2500	0.5	22.8	0.23	7	< 16.5	> 0.68

A resolution of better than about 100 μ is required at 20 TeV to make sensitive beam profile measurements (at the second pair of vertical bending magnets away from the high beta IR). Photon energies above about 50 eV are required. If the horizontal dipoles are used, about 250 eV would be required. With $E_c = 285$ eV, the flux should be adequate. At 1 TeV the resolution requirement is better than about 500 μ. Photon energies of about 3 eV or greater are required, but with critical energy 100 times smaller, the flux is neglible. One-TeV beam profiles cannot be obtained from central field sychrotron radiation.

G. Edge-Field Beam Profile Resolution Limits:

The diffraction limits are as above except that the form factors, which we label F_{eS}^B and F_{eS}^N, may be somewhat different. The depth of field and curvature distortions are related to L, the edge-field length parameter, instead of an arc length $\rho\theta$. The approximate measures and the rms spread caused by diffraction are shown in the following table.

| | $\theta_{eS} \ll \theta_{GB}$ | $\theta_{eS} \ll \theta_{GB}$ | $\theta_{eS} \gg \theta_{GB}$ | $\theta_{eS} \gg \theta_{GB}$ |
	$\theta_{eS} \ll \theta_{GN}$	$\theta_{eS} \gg \theta_{GN}$	$\theta_{eS} \ll \theta_{GN}$	$\theta_{eS} \gg \theta_{GN}$
$\rho\theta$	L	←same	L	←same
σ_{dif}^B	$0.5 F_{eS}^B L\theta_{eS}$	←same	$0.5 F_{eS}^B L\theta_{eS}\left(\frac{F^B\theta_{eS}}{F_S^B\theta_{GN}}\right)$	←same
σ_{curv}^B	$0.0745 L^2/\rho_0$	←same	$0.0745 L^2/\rho_0$	←same
$\sigma_{d.f.}^B$	$0.204 L\theta_{eS}$	←same	$0.204 L\theta_{GB}$	←same
σ_{dif}^N	$0.5 F_{eS}^N L\theta_{eS}$	$0.5 F_{eS}^N L\theta_{eS}\left(\frac{F^N\theta_{eS}}{F_{eS}^N\theta_{GN}}\right)$	$0.5 F_{eS}^N L\theta_{eS}$	$0.5 F_{eS}^N L\theta_{eS}\left(\frac{F^N\theta_{eS}}{F_{eS}^N\theta_{GN}}\right)$
$\sigma_{d.f.}^N$	$0.204 L\theta_{eS}$	$0.204 L\theta_{GN}$	$0.204 L\theta_{eS}$	$0.204 L\theta_{GN}$

The curvature distortion is smaller than the depth of field distortion provided $\theta_{eS} > (0.0745/0.204)L/\rho_0 = 4\mu r$ for the horizontal dipoles and $8\ \mu r$ for the vertical. This condition is well satisfied. As in the constant-field case, resolution is optimum when the geometrical aperture exceeds the limit set by θ_{eS}. Curiously though, the depth-of-field and diffraction spreads then become virtually identical: $F_{eS}(L/2)\theta_{eS}$ and $(1/\sqrt{6})(L/2)\theta_{eS}$. Typical values are shown below for p = 30 meters. The diffraction spread with $F_{eS} = 0.34$ and the depth-of-field σ's are combined in quadrature.

E_γ (eV)	λ (nm)	θ_{eS} (μr)	L (mm)	$\sigma_{dif}^{B(N)}$ (μ)	a_B, a_N (mm)	$\sigma_{\Delta z}$ (μ)
2.5	500	3922	65	67	> 117.7	400
		(2663)	(141)	(100)	(> 80.0)	(271)
25	50	1240	65	21	> 37.2	127
		(842)	(141)	(31)	(> 25.3)	(86)
250	5	392	65	7	> 11.8	40
		(266)	(141)	(10)	(> 8.0)	(27)
2500	0.5	124	65	2	> 3.7	13
		(84)	(141)	(3)	(> 2.5)	(9)

The rms deviation resolution of 67 (100) μ for optical frequencies is not

attainable because of the very large lens aperture required, $> 117.7(80.0)$ mm. However, the resolution can be relaxed at 1 TeV to a still very useful 500 μ by reducing the lens aperture to about 10 mm. A similar compromise can be found to obtain the required resolution at 20 TeV, but photon energies of greater than about 30 eV are required.

A resolution contribution peculiar to edge-field radiation occurs when the separation between the field entrance and the previous field exit is small enough that the images of entrance- and exit-field sources overlap to produce a depth of field effect. The circle of confusion has size $(\Delta z/2)\theta_{eS}$ with

$$\sigma_{\Delta z} = 0.204\Delta z\theta_{eS}.$$

As shown in the last column of the above table, this is a more serious limit than the diffraction limit unless the lens aperture is reduced as described above. On the other hand it is avoided in the vertical bending pair second from the high beta IR.
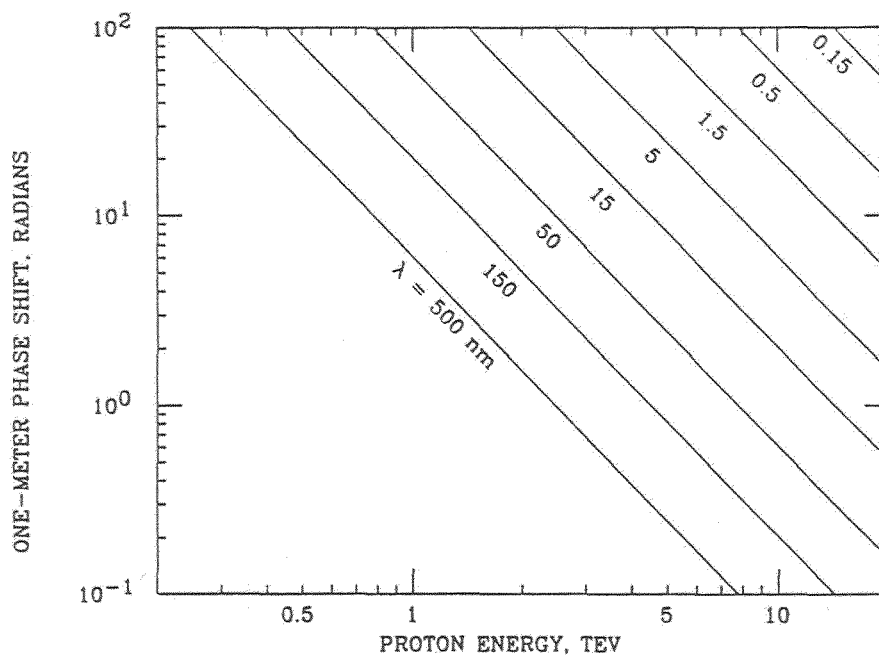
When the exit and entrance field radiation sources do overlap, constructive and destructive interference can occur depending upon the wavelength. A phase shift between the separated sources (which are coherent for the same particle) is caused by the fact that the particle traverses the gap more slowly than does light. Figure 11 shows the phase shift as a function of beam energy for a typical set of wavelengths for a one meter gap between exit and entrance edge fields. Note, however, that if the second pair of vertical magnets away from the high beta IR's is used, the exit and entrance edge field sources are so distant that their images are easily distinguished.

H. Summary and Conclusions.

The simple conclusion is that optimum resolution is obtained when the geometrical apertures in and normal to the bend plane, θ_{GB} and θ_{GN}, are somewhat larger than the natural synchrotron radiation opening angle θ_S for the constant-field source or θ_{eS} for the edge-field source. An adequate horizontal and vertical

resolution can be obtained for 1 TeV beam energy by imaging edge-field synchrotron radiation with optical devices. However, at 20 TeV, vacuum-ultraviolet or soft X-ray instrumentation is required.

This report has been more elaborate than the simple conclusions might seem to require. However, the detailed synchrotron-radiation beam profile measurements are can be achieved only by careful compromise. Furthermore, there is confusing literature on the subject. In a paper on a beam profile monitor for the NSLS VUV ring[9] the horizontal optics is said to be optimized by equating

11. Edge-field radiation phase shift over a one-meter distance from the exit edge-field region of one dipole to the entrance edge-field region of the next.

curvature distortion and diffraction size to obtain $\theta_{GB} = 2(\lambda/\rho)^{1/3}$. This does not consider the limiting effect of θ_S on the curvature distortion or diffraction, and is contrary to the conclusion drawn here.

The best place to make sensitive vertical and horizontal beam-profile measurements is probably with the second pair of vertical bending magnets away from the high beta IR's. This is a location of relatively large rms beam size, about 1000 μ to 230 μ for 1 to 20 TeV in both transverse directions, with lengthy straight sections on either side. At 1 TeV, edge-field radiation is required and, although optimum resolution requires excessively large lens apertures, perhaps 500 μ resolution can be obtained at optical frequencies for a 10 mm lens. At 20 TeV, good resolution cannot be obtained for sensitive beam profile measurement by using optical frequencies. Photon energies above about 30 eV (wavelengths less than about 40 nm) are required for edge-field radiation for reasonable lens aperture and above about 250 eV (wavelengths less than 5 nm) for the more familiar constant-field radiation.

Chromatic aberation has not been considered in this Part I. Its effect depends upon the choice of photon energy and upon the nature of the focusing system and detector and will therefore be deferred to Part III.

Edge-field synchrotron radiation from protons was first observed at the CERN SPS[7] when the intensity was successfully tracked for 280 to 400 GeV protons. A beam profile monitor was developed[10] for optical frequencies with a mirror, lens, and Vidicon of Intensified Silicon Target type (ISIT) detector. Useful beam diagnostics were established, such as measurement of the influence of a kick applied to the beam over one SPS revolution and of the emittance blowup due to proton scattering on residual gas during a coast of several hours at 270 GeV. To enhance synchrotron light for antiproton beams at the SP$\bar{\text{P}}$S, CERN[11] used in place of edge-field radiation an undulator, improved optics, and a detector consisting of a micro-channel image intensifier followed by a very sensitive ISIT.

The higher energies and beam currents at SSC provide a useful sensitivity

from edge- or constant-field synchrotron radiation and undulators may not be necessary. The same undulator that is tuned for visible light at the SP$\bar{\text{P}}$S would produce 12-keV X-rays from 20 TeV SSC beams! Alternatively, if tuned to visible light at 20 TeV, a five-period undulator would have to be 2.4 km long! However, a five period undulator for visible light would be 5.3 m for the 1 TeV case and may deserve further investigation.

REFERENCES

1. J.D. Jackson, *Classical Electrodynamics*.

2. Conceptual Design Report (CDR), SSC Central Design Group, SSC-SR-2020, March, 1986.

3. J.D. Jackson plans to change his text's definition by a factor of 1/2 to this conventional form in his next edition.

4. R. Coisson, Nucl. Instr. & Meth. *143*, 241 (1977) and R. Coisson, Phys. ReV. A, *20*, 524 (1979).

5. A. Hofmann, IEEE Trans. on Nucl. Sci., Vol NS-28, No. 3(1981).

6. Private Communication, Bill Gilbert *via* Dave Jackson. If we scale by bore, 3.45 cm to 7.5 cm, the vertical $L = 14.1$ cm.

7. R. Bossart, et al., Nucl. Instr. & Meth. *164*, 375 (1979).

8. estimated from $\sigma_\theta = \text{FWHM}/2.35$, where the full width at half maximum is determined by $sin^2\beta/\beta^2 = 0.5$, $\beta = \pi\alpha a/\lambda$, $\alpha = FWHM/2$, a being the slit width.

9. R. Nawrocky, J. Galayda, L. Yu and D. Shu, IEEE Trans. on Nucl. Sci. *NS-32*, 1893 (1985).

10. R. Bossart, et al., Proceedings of the 11th International Conference on High Energy Accelerators, Geneva (1980).

11. J. Bosser, et al., IEEE Trans. on Nucl. Sci. *NS-30*, 2164 (1983).